Covariance mapping of two-photon double core hole states in C2H2 and C2H6 produced by an x-ray free electron laser

M. Mucke, V. Zhaunerchyk, L. J. Frasinski, R. J. Squibb, M. Siano, J. H. D. Eland, P. Linusson, P. Salén, P. V D Meulen, R. D. Thomas, et al.

Covariance mapping of two-photon double core hole states in C_2H_2 and C_2H_6 produced by an x-ray free electron laser

New Journal of Physics

PAPER

CrossMark

Covariance mapping of two-photon double core hole states in C_2H_2 and C_2H_6 produced by an x-ray free electron laser

M Mucke[1], V Zhaunerchyk[1,2,3], L J Frasinski[4], R J Squibb[1,2,4], M Siano[4], J H D Eland[1,5], P Linusson[3], P Salén[3], P v d Meulen[3], R D Thomas[3], M Larsson[3], L Foucar[6,7], J Ullrich[8,9], K Motomura[10], S Mondal[10], K Ueda[10], T Osipov[11], L Fang[11,12], B F Murphy[11], N Berrah[11,13], C Bostedt[14], J D Bozek[14,15], S Schorb[14], M Messerschmidt[14,16], J M Glownia[14], J P Cryan[14], R N Coffee[14], O Takahashi[17], S Wada[18], M N Piancastelli[1,19], R Richter[20], K C Prince[20] and R Feifel[1,2,21]

1   Department of Physics and Astronomy, Uppsala University, Sweden
2   Department of Physics, University of Gothenburg, Sweden
3   Department of Physics, AlbaNova University Center, Stockholm University, Sweden
4   Department of Physics, Imperial College London, UK
5   Department of Chemistry, Oxford University, UK
6   Advanced Study Group of the Max Planck Society, Hamburg, Germany
7   Max Planck Institut für medizinische Forschung, Heidelberg, Germany
8   Max Planck-Institut für Kernphysik, Heidelberg, Germany
9   Physikalisch-Technische Bundesanstalt, Braunschweig, Germany
10   Institute for Interdisciplinary Material Research, Tohoku University, Sendai, Japan
11   Department of Physics, Western Michigan University, Kalamazoo, MI, USA
12   Center for High Energy Density Science, University of Texas, Austin, TX, USA
13   Department of Physics, University of Connecticut, Storrs, CT, USA
14   SLAC National Accelerator Laboratory, Menlo Park, CA, USA
15   Science Division, Synchrotron SOLEIL, Gif-sur-Yvette, France
16   NSF BioXFEL Science and Technology Center, Buffalo, NY, USA
17   Institute for Sustainable Science and Development, Hiroshima University, Japan
18   Department of Physical Science, Hiroshima University, Japan
19   Laboratoire de Chimie Physique, Matière et Rayonnement (LCPMR), UPMC, Université Paris 06, and CNRS (UMR7614), Paris Cedex, France
20   Elettra-Sincrotrone Trieste, Basovizza, Italy
21   Author to whom any correspondence should be addressed.

E-mail: raimund.feifel@physics.gu.se

Abstract

Few-photon ionization and relaxation processes in acetylene (C_2H_2) and ethane (C_2H_6) were investigated at the linac coherent light source x-ray free electron laser (FEL) at SLAC, Stanford using a highly efficient multi-particle correlation spectroscopy technique based on a magnetic bottle. The analysis method of covariance mapping has been applied and enhanced, allowing us to identify electron pairs associated with double core hole (DCH) production and competing multiple ionization processes including Auger decay sequences. The experimental technique and the analysis procedure are discussed in the light of earlier investigations of DCH studies carried out at the same FEL and at third generation synchrotron radiation sources. In particular, we demonstrate the capability of the covariance mapping technique to disentangle the formation of molecular DCH states which is barely feasible with conventional electron spectroscopy methods.

1. Introduction

Experiments using x-ray free electron lasers (FELs) have opened up extraordinary opportunities in many scientific areas. One topic of great interest, with potential impact on fields such as bio-imaging and materials science, is double core hole (DCH) spectroscopy, which was first proposed theoretically by Cederbaum and coworkers in the mid 1980s [1, 2]. Experimental study in this field has been greatly enhanced by the world's first

hard x-ray FEL source, the linac coherent light source (LCLS) at the SLAC National Accelerator Laboratory, Stanford, USA. Two basic cases can be distinguished: either both core holes reside on the same atom, a state denoted as single-site (ss) DCH, or the two core vacancies are located on two different atoms of the molecule, which is referred to as two-site (ts) DCH. The numerical studies suggest in particular that the ts-DCH states should be far more sensitive to the chemical environment than the single core hole (SCH) states [1, 2], already widely studied by conventional x-ray photoelectron spectroscopy also known as 'electron spectroscopy for chemical analysis (ESCA)' [3].

Early FEL experiments on Ne were carried out by Young and coworkers [4], on N_2 by Cryan and coworkers [5] and by Fang and coworkers [6], and from these studies DCH states were known to be efficiently created at the LCLS by sequential x-ray two-photon absorption. Subsequent experiments using the same detection technique as in [4–6] improved the data quality and gave first insights into ts-DCH states [7, 8].

At the same time as the recent FEL work, DCH states have also been studied in synchrotron radiation-based experiments using a highly efficient multi-electron coincidence spectroscopy technique based on a magnetic bottle [9–15]. It is known from related multi-electron coincidence experiments [16–18], that the advantage of using a multi-particle correlation method compared with a single particle detection scheme as used in [4–8] lies in the fact that one accesses the inherent correlation of particles originating from the same ionization event. In this way one can retrieve the signals of interest, which otherwise may overlap with other signals. It should be noted that in synchrotron radiation experiments, ss-DCH states are formed far more easily than the ts-DCH states [12] due to the single-photon excitation character of this light source, whereas at an FEL the two types of DCH states are expected to be equally accessible by two-photon absorption. From simple population arguments one can expect for the present C_2H_2 and C_2H_6 cases that in using the two-photon route the formation of ts-DCHs should be twice as likely as that of ss-DCHs since upon removal of the first electron, two core electrons are still available on the second, non-ionized core, while only one electron is left on the already ionized core. The two-photon route is nonlinear, since the spectral intensity scales with the square of the photon flux density and like many nonlinear processes it requires extremely high irradiance which can be obtained by tight focusing of the light beam.

However, studies of DCH states at an FEL including their decay pathways are complicated by interference from alternative multi-ionization pathways involving inner-shell levels. In principle, the decay routes of DCH states are known in terms of a theoretical model commonly used for predicting the final charge states [19]. Within this model, one distinguishes the interfering PAP process from the interesting PPA process, where P stands for photoelectron and A stands for Auger electron and the sequence of letters represents the sequence of processes. In the case of a PAP process, the first x-ray photon ionizes the core shell, which is then refilled by a valence electron, with simultaneous ejection of an Auger electron before the second x-ray photon ejects another core electron. In contrast, in the PPA process the second core electron is ionized immediately after the first core-shell ionization and prior to the occurrence of Auger decay, so forming a DCH state. The competition between the different pathways depends on the x-ray pulse duration relative to the core hole lifetime, which is about 7 fs [20] for carbon-containing molecules. This means that in order to enhance the probability of the DCH (PP) process, a pulse length comparable to the core hole lifetime is of great advantage, since then the second x-ray photon is likely to be absorbed by the singly-ionized core-hole state prepared by the first x-ray photon, rather than by the state formed by Auger decay of the initial single-hole state [22]. We also note in this context that recent theoretical calculations [23] predict a much shorter lifetime for ss-DCH than for ts-DCH, with a difference larger than a factor of two.

The present work advances earlier DCH FEL studies by introducing the capability to detect multiple electrons concurrently, so determining their inherent correlations. To do this, the technique of covariance mapping, originally introduced to the field of photoionization by Frasinski and coworkers [21], is utilized. This statistical analysis technique overcomes the drawback of the low FEL repetition rate for establishing the correlations between multiple particles. The results are equivalent to true coincidences, and remove ambiguities in assigning features which may be blurred or overlapped in one-dimensional spectra.

2. Experimental details

Experiments were carried out at the atomic, molecular and optical (AMO) science instrument [24, 25] at the LCLS at SLAC, Stanford. The LCLS was operated in its 20 pC low-charge mode and at a repetition rate of 120 Hz, where the FEL pulses were tuned to nominally 5 fs length and about 0.1 mJ energy. The central photon energies were determined off-line from machine parameters as approximately 499 eV for the C_2H_2 measurements and about 500 eV for the C_2H_6 recordings. Four gas detectors, which are routinely available at the AMO instrument, were used to monitor the LCLS pulse energy on a shot-by-shot basis. In the present experiments, the x-ray pulse energy was found to vary by about 15%. The pulses were focused by a pair of elliptically bent Kirkpatrick-Baez

mirrors into the light–matter interaction region of the High Field Physics (HFP) chamber of the AMO instrument, and the FWHM diameter of the focused beam was estimated to be $\sim 1.4\,\mu$m or less.

The HFP chamber of the AMO instrument was equipped with our custom-made magnetic bottle spectrometer FELCO, developed on the design principles of previous work [16, 26] specifically to perform multi-electron correlation studies at FEL sources. Briefly, the spectrometer consists of a strong permanent magnet of conical shape which is located close to the light–matter interaction region and whose divergent magnetic field collects all electrons created in ionization and directs them into a drift tube about 2 m long. The tube is surrounded by a solenoid to create a homogeneous weak magnetic field that guides the electrons towards a multi-channel plate detector in a Chevron configuration installed at the end of the flight tube. This spectrometer type is characterized by a high collection efficiency of more than 90% of the whole 4π solid angle, implying a total collection-detection efficiency for single electrons of $\approx 50\%$. A stack of electrostatic lenses was installed at the entrance of the drift tube allowing either retardation of high kinetic energy electrons to improve the spectral resolution, or efficient ion detection (see [27, 28]). Mass spectra were recorded in this mode to check sample purity and to evaluate light-intensity dependent fragmentation patterns of the molecules.

The sample gas was introduced into the experimental chamber through an Even Lavie valve [29, 30] operated at 120 Hz repetition rate with an opening time of 24 μs. The gas beam passed a conical skimmer of 200 μm diameter before reaching the interaction region of the spectrometer where it was crossed perpendicularly by the horizontally polarised FEL beam. In order to avoid clustering, commercially available acetylene (C_2H_2) and ethane (C_2H_6) of purity > 99% was diluted with helium in an external cylinder, and the Even Lavie valve was heated to approximately 80°C.

Time-of-flight (TOF) electron signals were recorded, for every LCLS shot, as complete wave forms using a transient digitizer and sent to a fast data storage system. Each shot could contain as many as ~ 50 electron signals. The spectra were converted from flight time to kinetic energy (E_{kin}) according to

$$E_{\text{kin}} = \frac{D_0^2}{(t - t_0)^2} + E_0, \tag{1}$$

where t denotes TOF and D_0, t_0 and E_0 are conversion and calibration factors. A typical data set consists of about 500 000 shots corresponding to a data acquisition time > 1 h at 120 Hz repetition rate.

Online analysis of the TOF data as well as the data converted to a kinetic energy scale was performed [31, 32] to quickly assess the data quality. To visualise the correlations between the electrons, the statistical method of covariance mapping [21], which principle has already been deployed in related investigations at the FEL on the Ne atom [32, 34], is employed. Briefly, two-dimensional covariance maps are constructed by calculating the difference between the correlated $\langle XY \rangle$ and the uncorrelated $\langle X \rangle \langle Y \rangle$ products of electron signals X and Y at two kinetic energies within the same single-shot waveform for all possible energy pairs according to
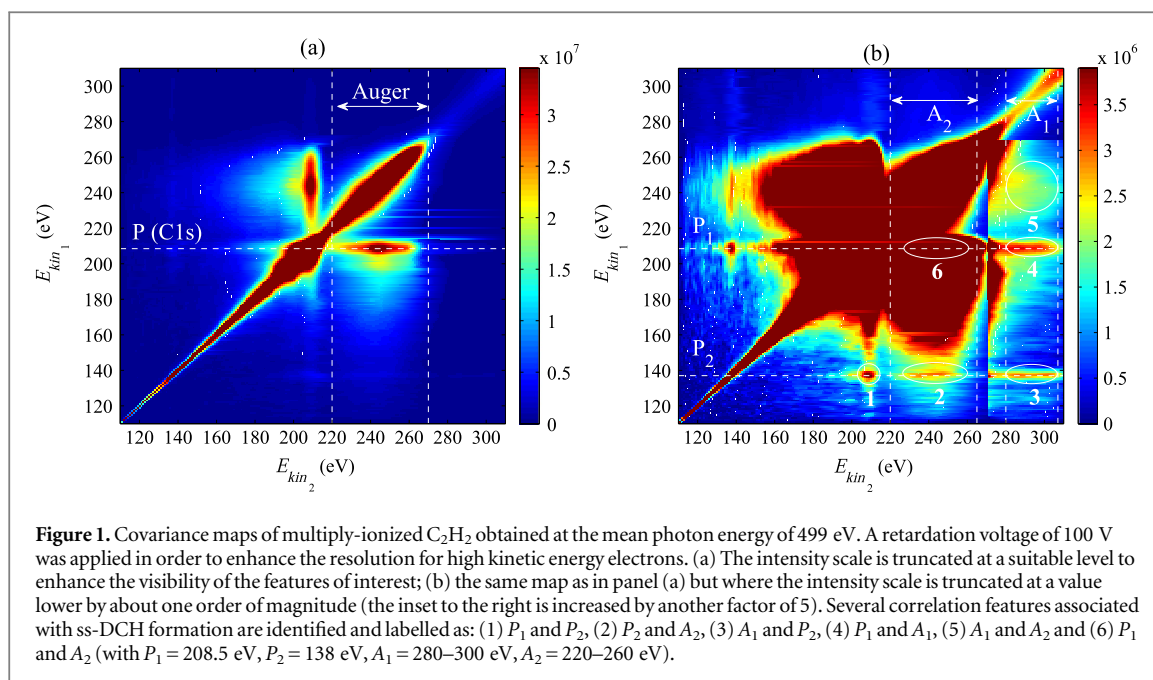
$$\text{Cov}(X, Y) = \langle XY \rangle - \langle X \rangle \langle Y \rangle, \tag{2}$$

where terms in angled brackets $\langle ... \rangle$ denote the average over all shots. The covariance intensities are plotted as a two-dimensional map against the kinetic energies of the two electrons at each point. Such maps show pairwise correlations, but as each of the events of interest (PAPA, PPAA etc) typically produces four electrons of different energies, each type of event is expected to produce six features in the maps. Because signals are measured at a single detector, the maps are completely symmetrical about the leading diagonal.

In the off-line analysis, the standard covariance technique [21] was enhanced in several ways in order to improve the quality of the maps. To begin with, a jitter correction was implemented in order to account for shot-by-shot fluctuations of the photon energy. For every shot, the photon energy was determined from the FEL beam parameters and the kinetic energy scales of the spectra were calibrated accordingly; this led to sharper photoelectron lines when averaged over many shots, but at the expense of somewhat broadened Auger lines. Secondly, the variation in light intensity from shot to shot was compensated, first by partial covariance [32, 34] and later by the method of contingent covariance mapping [33], where data from shots of similar intensity were analyzed in groups and their covariance maps were subsequently combined. A more detailed description of our enhanced analysis procedure is given by Zhaunerchyk *et al* [34].

3. Theoretical details

Molecular geometries of C_2H_2 and C_2H_6 were calculated by geometry optimization at the MP2/cc-pVTZ level of theory using the Gaussian 09 suite of programs [38]. The single and double core ionization potentials (SIP and DIP) of the SCH, ss-DCH, and ts-DCH states of the molecules were estimated using the MCSCF method [39] with cc-pCVTZ basis sets of Dunning [42, 43]. Computational details have been described elsewhere [36, 44]. We used the active space comprising all occupied molecular orbitals (except the 1s orbitals of the carbon atoms)

Figure 1. Covariance maps of multiply-ionized C_2H_2 obtained at the mean photon energy of 499 eV. A retardation voltage of 100 V was applied in order to enhance the resolution for high kinetic energy electrons. (a) The intensity scale is truncated at a suitable level to enhance the visibility of the features of interest; (b) the same map as in panel (a) but where the intensity scale is truncated at a value lower by about one order of magnitude (the inset to the right is increased by another factor of 5). Several correlation features associated with ss-DCH formation are identified and labelled as: (1) P_1 and P_2, (2) P_2 and A_2, (3) A_1 and P_2, (4) P_1 and A_1, (5) A_1 and A_2 and (6) P_1 and A_2 (with $P_1 = 208.5$ eV, $P_2 = 138$ eV, $A_1 = 280$–300 eV, $A_2 = 220$–260 eV).

and all unoccupied valence orbitals which contain large contributions from different atomic s and p orbitals, with core occupancy being fixed. More explicitly, the size of the active space in the present study consists of 10 electrons distributed in 12 orbitals for C_2H_2 and of 14 electrons distributed in 16 active orbitals for C_2H_6. For computational economy, the number of configurations was limited; only singly and doubly excited configurations were included in the MCSCF calculations for C_2H_6. Note that the core hole orbitals were frozen in all the CASSCF calculations. The DIPs were calculated using the localized molecular orbital picture. Only the core orbitals were localized, which was done using the Boys method [40]. The CASSCF calculations were performed with the MOLPRO2012 quantum chemistry package [41].

4. Results and discussion

4.1. C_2H_2 case

Figure 1 shows covariance maps for C_2H_2 ionized at a mean photon energy of 499 eV. For measurement of this data, a retardation voltage of 100 V was applied to increase the resolution for high kinetic energy electrons. The intensity scale of the (same) map(s) is truncated at two different levels to enhance visibility of the major features, in the presence of the very strong diagonal line at equal kinetic energies, due to the autocorrelation signal. The line structure visible in figure 1(a) at 208.5 eV corresponds to the primary C1s single ionization process. The associated island in the energy pair region of $\approx$ 205–213 eV and 220–270 eV shows the expected correlation between the C1s photoelectron and the subsequent normal Auger electron emission.

By truncating the intensity scale at a level lower by about one order of magnitude than the level used for figure 1(a), we make weaker correlation signals discernible in figure 1(b). To identify the features observed we make use of the energies expected for the possible processes such as PPA(A) or PAP(A) based on known [45] or here measured and calculated ionization potentials; because the two Auger electrons can have similar energies with a broad spread, and are not always experimentally distinguishable, we generally retain the symbols A and P up to the last detected electron of interest. After a first core ionization, the energy of a new photoelectron produced by a second photon hitting the same molecule will depend on whether the second interaction happens at the already ionized atom or at another atom of the same molecule. This energy difference, due to differences in the Coulomb interactions, distinguishes ss-DCH and ts-DCH formation. In ss-DCH formation the second ionization energy will be significantly higher than the first and the kinetic energy of the second photoelectron will be correspondingly lower, because the interaction involves one and the same carbon atom, whereas in the case of ts-DCH, the second photon interacts with an ionized system where the Coulomb potential is localised at the other carbon atom. The shift in ionization potential is therefore much reduced, and comparable to that between a neutral and valence ionized molecule. The kinetic energy of the second emitted photoelectron will be only a little higher than that of the first. The Auger electron energies also depend strongly on the type of DCH state: the first Auger electron emitted from a ss-DCH state, the hypersatellite Auger electron, is expected to have the highest kinetic energy whereas for the first Auger electron emitted from a ts-DCH a significantly lower

Table 1. Theoretical and experimental values for electron energies from multi-ionization of C_2H_2; unreferenced values are from this work; the values presented in italic style are estimates based on known [45] or here measured and calculated ionization potentials; the values marked with an asterisk are theoretical values for the photon energy used in this work.

C_2H_2 $h\nu = 499$ eV		Theory from [36]	Theory from [13]	Theory	Experiment	E_{kin}-range projection
SCH P_1	E_{bin} (eV)			291.08	291.1 [37]	207–211
ss-DCH	E_{bin} (eV)	650.23	650.02	650.7	652.5 [13]	
- P_2	E_{kin} (eV)			139.4*		136–140
- A_1	E_{kin} (eV)			260–310 [45]	280–300	288–292
- A_2	E_{kin} (eV)			210–255 [45]	220–260	
ts-DCH	E_{bin} (eV)	594.59	595.86	594.9	596.0 [13]	
- P_2	E_{kin} (eV)			195.2*		193–197
- Augers	E_{kin} (eV)			225–245 [45]	220–270	
PA... -sequences						
- P_2	E_{kin} (eV)			180–191*		183–187
- A_2	E_{kin} (eV)			190–290	220–270	

kinetic energy range is expected. The first and second Auger electrons from a ts-DCH are in the same energy range as Auger electrons from a SCH state, 200–270 eV for C_2H_2 (see [12]). The second Auger electron from a ss-DCH and all the Auger electrons emitted in sequential processes such as PAP(A) are also expected to fall within essentially the same kinetic energy range. Thus the majority of the Auger electron signals are heavily overlapped and difficult to distinguish.

Many of the features observed in figure 1(b) can be assigned on the basis of the electron kinetic energies expected for the case of C_2H_2 ionized by 499 eV photons. The energies are known from theoretical work [13, 36, 37, 45] including our own calculations, and from experimental data [12, 13], as summarized in table 1. In particular, we identify all correlation islands associated with ss-DCH formation and subsequent Auger decays as follows: (1) P_1 and P_2, (2) P_2 and A_2, (3) A_1 and P_2, (4) P_1 and A_1, (5) A_1 and A_2, and (6) P_1 and A_2, where P_i denotes a photoelectron and A_j an Auger electron with the indices i, $j = 1$ and 2 labelling their emission order.

Figure 2 represents C_2H_2 data measured with a higher retardation voltage of 150 V. At 195 eV, the kinetic energy expected for the second photoelectron from a ts-DCH process, we see a correlation with the Auger electron range of 220–270 eV marked as island 7 in figure 2. In addition there is a correlation between the 195 eV feature and the main photoelectron line at ≈ 208 eV. We note that 195 eV is also an energy where satellites of the main C1s photoelectron line are expected to be located, approximately 12 eV below the main C1s line [37], but those satellites should not correlate with the C1s line.

In order to check our assignment versus sequential processes of the PAPA...type, we performed calculations which suggest that the second and later photoelectrons from such a sequence have substantially lower kinetic energies than the second photoelectron from ts-DCH; the second photoelectron is expected to be between 180 and 191 eV, and subsequent ones even lower. Indeed, in figure 2 we observe a correlation feature along the kinetic energy of 185 eV marked as island 8 in figure 2. This supports our assignment of the correlation feature at the higher energy pair 195 and 208 eV with the formation of a ts-DCH.

To examine the correlation between the different electron pairs more quantitatively, figure 3 (a) shows in panels (1)–(5) projections of the covariance map in the following selected kinetic energy ranges (the corresponding electron on which the selection is based is marked in bold face): (1) 288–292 eV (ss − P**PA**, i.e. A_1 from ss-DCH), (2) 136–140 eV (ss − P**PA**, i.e. P_2 from ss-DCH), (3) 183–187 eV (PA**P**, i.e. P_2 from a sequential ionization process), (4) 207–211 eV (**P**PA/**P**AP, i.e. P_1 from SCH, DCH or sequential processes), and (5) 193–197 eV (ts-P**PA**, i.e. P_2 from ts-DCH). In panel (6) of figure 3 (a), a core level photoelectron spectrum including normal Auger transitions based on the summation of single-shot spectra is given; this corresponds to what can be measured by conventional ESCA and Auger electron spectroscopy. For comparison, an Auger spectrum produced by C1s ionization of acetylene taken from the literature [35] has been added in panel (7),
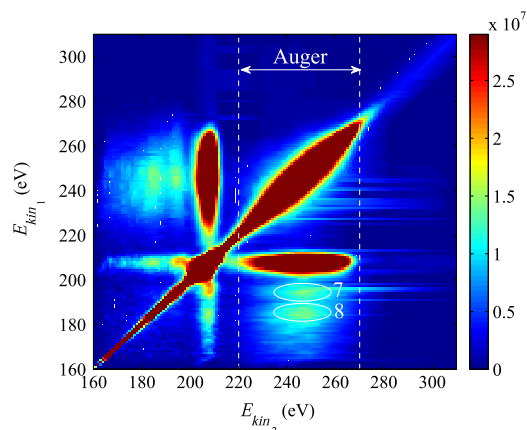
Figure 2. Covariance map of C_2H_2 obtained at the mean photon energy of 499 eV and with a retardation of 150 V. Two correlation islands, 7 and 8, along the kinetic energies of 195 and 185 eV, respectively, are marked and are discussed further in the text. The very intense feature located above islands 7 and 8 and within the kinetic energy range of 220–270 eV is associated with normal Auger decay of the single core hole.
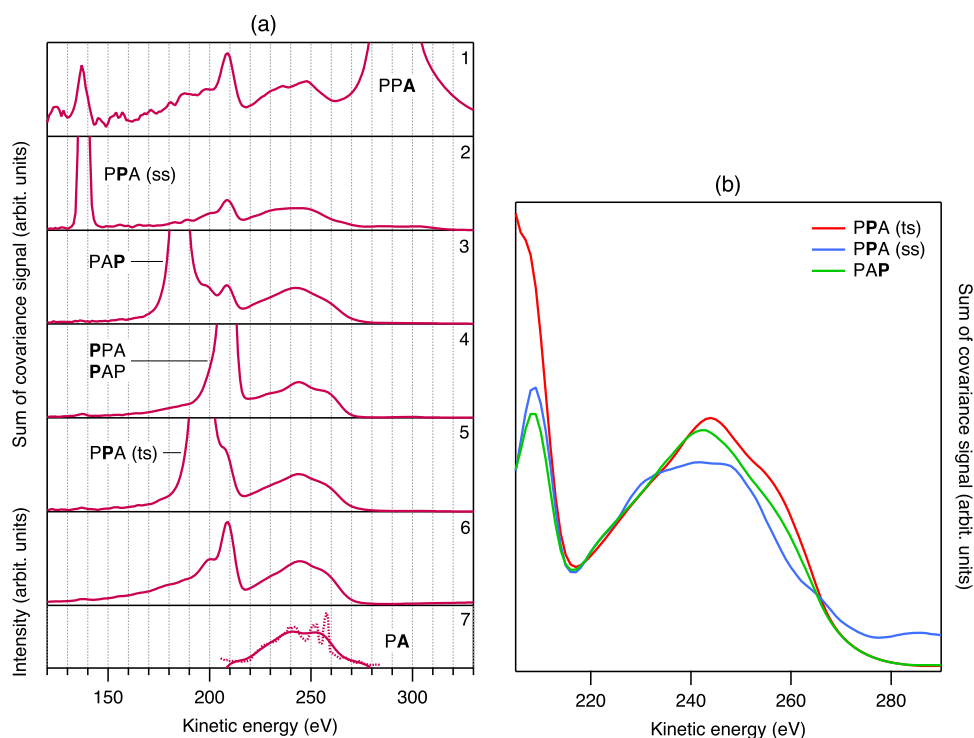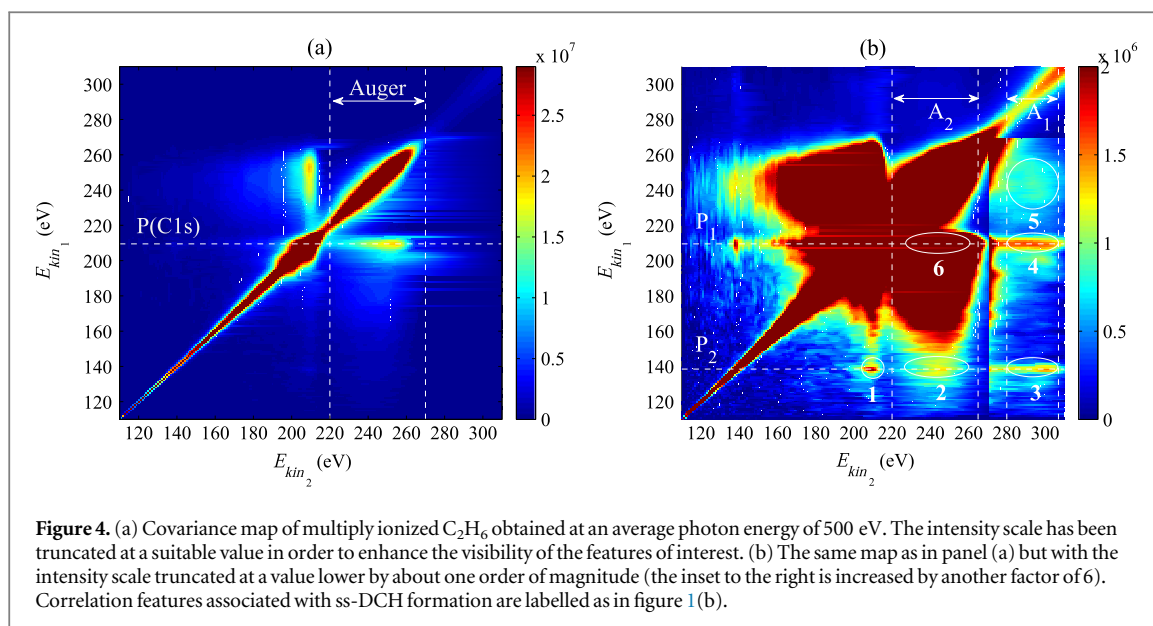

Figure 3. (a) Projections of the C_2H_2 covariance map (see figure 1) selected at the kinetic energy ranges: (1) 288–292 eV (ss − PP**A**), (2) 136–140 eV (ss − P**P**A), (3) 183–187 eV (PA**P**), (4) 207–211 eV (**P**PA/**P**AP), and (5) 193–197 eV (ts − PP**A**). Panel (6) displays a conventional core level photoelectron spectrum including normal Auger transitions and panel (7) shows the normal Auger spectrum of C_2H_2 taken from the literature [35], both in its original form (dashed line) and in the form of a convolution of this spectrum with a Gaussian of 4 eV FWHM equal to the energy resolution of our experimental data; (b) the same data as in panels (2), (3) and (5) of (a) but where the energy scale comprises the Auger region only and where the relative intensities are rescaled for direct comparison.

both in its original form (dashed line) and in the form of a convolution of this spectrum with a Gaussian of 4 eV FWHM equal to the energy resolution of our experimental data.

The projections in the first five panels of figure 3 (a) show strong maxima at the positions where the autocorrelation appears; they have been cut off in intensity to enhance the visibility of weaker features. The projection for the hypersatellite Auger electron in panel (1) shows strong correlations with the first photoelectron (about 208.5 eV), with the second photoelectron from ss-DCH (about 138 eV), as well as with the energy range of the second Auger electrons emitted (220–260 eV). This is expected since all these features are fingerprints of the ss-DCH process. The same holds for the correlation of the second photoelectron

Figure 4. (a) Covariance map of multiply ionized C_2H_6 obtained at an average photon energy of 500 eV. The intensity scale has been truncated at a suitable value in order to enhance the visibility of the features of interest. (b) The same map as in panel (a) but with the intensity scale truncated at a value lower by about one order of magnitude (the inset to the right is increased by another factor of 6). Correlation features associated with ss-DCH formation are labelled as in figure 1(b).

from ss-DCH, as shown in panel (2), whose energy is very well separated from all the others. This is the only electron whose correlation with the hypersatellite Auger region (about 280–300 eV) is clear, though the feature is relatively weak, possibly due to reduced detection efficiency for such high kinetic energy electrons. In theory, the correlated intensities for all features in the maps representing single processes, such as ss-DCH formation, should be equal. In practice the relative intensities are hard to extract because of overlapping features and a structured background level, stemming from the tails of the autocorrelation line. The two clearest features P_2 and P_1(C1s) and P_2 and A_2 from ss-DCH formation in acetylene have the same apparent intensities within a factor of 2, which is consistent with the assignment.

The correlation spectrum shown in panel (3) of figure 3 (a) focuses on the energy region where the second photoelectron from a PAP sequence is expected. Here a strong correlation with the main photoelectron as well as the main Auger region can be observed, while there is no correlation with any hypersatellite Auger electrons. For further comparison, panel (4) shows correlation signals associated with the P_1 electron, which is ejected in all processes initiated by primary C1s ionization. Therefore this projection reflects a combination of the correlation features discussed so far. It also contains the comparatively strong correlation feature based on the conventional SCH ionization process and on the normal Auger decay, which dominates the comparatively weak signals for electrons stemming from few-photon processes. As expected the features assigned to this PAP process have considerably higher relative intensity than those representing ss-DCH formation.

On examining the Auger bands in the different panels of figure 3 (a) more closely, we notice substantial changes in their shape and shifts in their centre of mass. As can be seen from figure 3 (b), the second Auger electron emitted from a ss-DCH contributes more in the low kinetic energy range of this Auger region than other competing processes. In contrast, a well pronounced shoulder at around 260 eV is discernible in the projection associated with ts-DCH formation and is attributed to the emission of firstly emitted Auger electrons (A_1). Also, as can be seen from the projection associated with (PA)$_n$ sequence, A_1 Auger electrons originating from those processes contribute to the same kinetic energy region, but with a distinctly different intensity distribution. Similarly distinct intensity distributions for the projections associated with ts-DCH, ss-DCH and (PA)$_n$ processes, respectively, are observed in the kinetic energy region around 240 eV which is primarily attributed to their secondly emitted Auger electrons (A_2). This might be regarded as suggesting that ts-DCHs are efficiently produced upon two-photon absorption, as predicted by the simple population argument mentioned in the introduction. Indeed, the one feature attributed above to ts-DCH formation appears to have an intensity that is at least comparable to any of the features of ss-DCH formation. A factor of 2 in intensity difference is expected on the basis of the number of K-electrons available for ionization in the two cases.

4.2. C_2H_6 case

Figure 4(a) shows the covariance map of multiply ionized C_2H_6 obtained at an average photon energy of 500 eV and presented in the same way as in figure 1(a). Again, the intensity scale has been truncated at a suitable value in order to enhance the visibility of the features of interest. As can be seen, the map for C_2H_6 is highly reminiscent of that for C_2H_2.

Table 2. Theoretical and experimental values for electron energies from multi-ionization of C_2H_6; unreferenced values are from this work; the values marked with an asterisk are theoretical values for the photon energy used in this work.

C_2H_6 $h\nu = 500$ eV		Theory from [36]	Theory from [13]	Theory	Experiment
SCH P_1	E_{bin} (eV)			290.5	
ss-DCH	E_{bin} (eV)	648.83	648.11	648.1	650.6 [13]
- P_2	E_{kin} (eV)			142.4*	
- A_1	E_{kin} (eV)				280–300
- A_2	E_{kin} (eV)				220–260
ts-DCH	E_{bin} (eV)	589.01	589.47	590.0	590.2 [13]
- P_2	E_{kin} (eV)			199.2*	
- Augers	E_{kin} (eV)				220–270

In order to enhance the weaker, few-photon excited correlation features of multiply ionized C_2H_6, we rescaled the intensity by about one order of magnitude compared with the scale used in figure 4(a). The corresponding map is shown in figure 4(b). As in the case of the C_2H_2 map, we can clearly identify all expected correlation features associated with ss-DCH formation which are labelled 1 to 6 following the same notation as was used for the labelling of the C_2H_2 data. In particular, the second photoelectron associated with the ss-DCH state appears at about 138.5 eV kinetic energy, the hypersatellite Auger electrons fall within the range of 280–300 eV, and the second emitted Auger electrons are found in the range of 220–260 eV. The experimental values extracted are given together with the corresponding theoretical values in table 2.
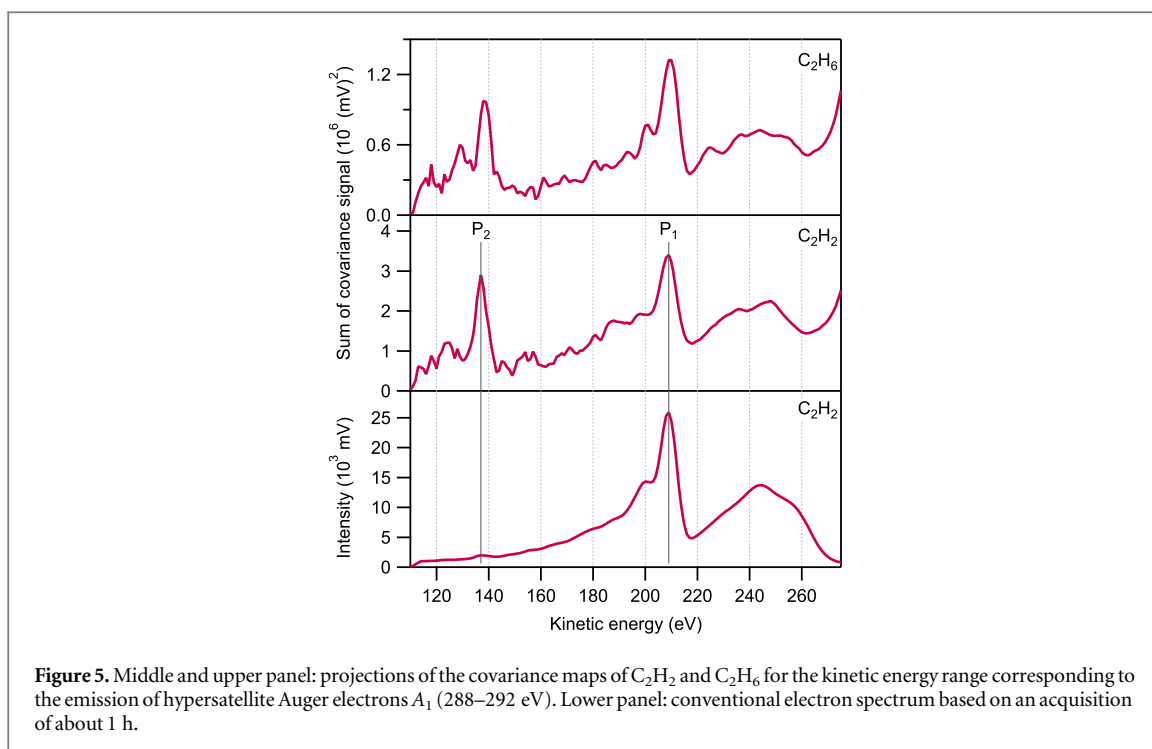
Identification of features associated with ts-DCH formation is more challenging for C_2H_6 than for C_2H_2 because the kinetic energy of the second photoelectron is expected to be less than 5 eV lower than the energy of the first emitted core electron. Since the resolution for photoelectrons is limited to the bandwidth of the FEL radiation plus the photon energy jitter, which are of the same order of magnitude, the signal of the second emitted photoelectron is overlapped by the wings of the main C1s photoelectron line.

4.3. Comparison of the covariance mapping technique with conventional photoelectron spectroscopy

Figure 5 presents in its middle and upper panel two projections of the covariance maps of C_2H_2 and C_2H_6 for the kinetic energy range corresponding to the hypersatellite Auger electron A_1 which is associated with a ss-DCH decay process and which, for energetic reasons, is well separated on the map from other features. The kinetic energy scale presented extends up to about 265 eV, deliberately excluding the otherwise dominant autocorrelation part. For both molecular systems, we observe strong correlations with not only the main photoelectron peak P_1 at around 208 eV kinetic energy, but also with the second photoelectron from the ss-DCH process P_2 at around 138 eV, as well as with Auger electrons within the range of 220–260 eV kinetic energy. The peak heights of the P_1 and P_2 features are nearly the same, supporting the interpretation that they are associated with a single process, namely formation and decay of ss-DCH states.

In order to illustrate the advantage of the covariance mapping technique, we included in the lower panel of figure 5 the conventional core electron spectrum of C_2H_2 based on an acquisition of about 1 h. Whereas in the one-dimensional spectrum there is hardly any clear peak structure associated with the P_2 electron from ss-DCH at around 138 eV kinetic energy, we can see a very strongly pronounced peak at this energy position in the corresponding projection of C_2H_2. This represents correlation between the second emitted photoelectron and the first Auger electron associated with ss-DCH creation. We note that the acquisition time for the data on which the projections are based was the same as for the conventional spectrum. We can thus conclude that an advantage of using the covariance mapping technique lies in the fact that it brings out features of interest more distinctly than conventional electron spectroscopy techniques.

This conclusion also holds for comparison with DCH detection in true coincidence mode with the same kind of magnetic bottle spectrometer at a synchrotron radiation source. As mentioned above, in the present work, we allowed for as many as 50 electrons for a single LCLS pulse, or for an estimated average of about 25 electrons per radiation pulse, which resulted in sufficiently good statistics within less than 1 h. Since the LCLS was operated at a repetition rate of 120 Hz, this amounts to an electron count rate of 3 kHz which is very similar

Figure 5. Middle and upper panel: projections of the covariance maps of C_2H_2 and C_2H_6 for the kinetic energy range corresponding to the emission of hypersatellite Auger electrons A_1 (288–292 eV). Lower panel: conventional electron spectrum based on an acquisition of about 1 h.

to what is typically used in synchrotron radiation based coincidence experiments using a magnetic bottle [9]. By examining on our covariance maps the volumes associated with SCH and ss-DCH formation, we obtain an estimate for the relative intensity ratio of the two processes of about 3%. In contrast, as mentioned in several synchrotron radiation based DCH works, the corresponding relative ratio is on the order of 10^{-3} [9, 12, 14, 15]. This implies that in order to obtain the same amount of ss-DCH signal at a synchrotron radiation source, data acquisition will need to take about 10 times longer. Furthermore, as discussed above, in the case of nonlinear FEL based experiments the formation of ts-DCH in comparison to ss-DCH can be expected to be of similar probability. In contrast, at synchrotron radiation sources, where primarily single-photon transitions are utilized, the cross-section for ts-DCH formation is known to be about two orders of magnitude lower than for ss-DCH formation [12], which implies that the data acquisition for good statistics ts-DCH signals requires several days at the storage rings.

5. Conclusions

Two-photon excited multi-ionization processes in acetylene and ethane have been successfully detected in short run times at the intense x-ray FEL beam of the LCLS at Stanford. By combining a multi-electron spectrometer of high collection-detection efficiency with the data analysis technique of covariance mapping. Signatures of both ss- and ts-DCH production could be identified, as well as those of some competing processes involving sequences of core ionization and Auger decay.

The measurements confirm the prediction that in DCH production by two-photon ionization using intense pulsed light, ts-DCHs and ss-DCHs are formed with comparable probabilities. Although the covariance analysis method alleviates some spectral congestion from competing processes, some still remains. This means that the technique still needs further development before it can be applied to larger molecules. In particular, even shorter light pulses of the order of 1 fs and more precise photon energy measurement and control would be highly advantageous.

Acknowledgments

References

[1] Cederbaum L S *et al* 1986 *J. Chem. Phys.* **85** 6513
[2] Cederbaum L S 1987 *Phys. Rev.* A **35** 622
[3] Siegbahn K *et al* 1971 *ESCA Applied to Free Molecules* (Amsterdam: North-Holland)
[4] Young L *et al* 2010 *Nature* **466** 56
[5] Cryan J P *et al* 2010 *Phys. Rev. Lett.* **105** 083004
[6] Fang L *et al* 2010 *Phys. Rev. Lett.* **105** 083005
[7] Berrah N *et al* 2011 *Proc. Natl Acad. Sci. USA* **108** 16912
[8] Salén P *et al* 2012 *Phys. Rev. Lett.* **108** 153003
[9] Eland J H D *et al* 2010 *Phys. Rev. Lett.* **105** 213005
[10] Lablanquie P *et al* 2011 *Phys. Rev. Lett.* **106** 063003
[11] Linusson P *et al* 2011 *Phys. Rev.* A **83** 022506
[12] Lablanquie P *et al* 2011 *Phys. Rev. Lett.* **107** 193004
[13] Nakano M *et al* 2013 *Phys. Rev. Lett.* **110** 163001
[14] Hedin L *et al* 2013 *J. Chem. Phys.* **140** 044309
[15] Hedin L *et al* 2014 *Chem. Phys.* **439** 111
[16] Eland J H D *et al* 2003 *Phys. Rev. Lett.* **90** 053003
[17] Feifel R *et al* 2006 *J. Chem. Phys.* **122** 144308
[18] Eland J H D *et al* 2005 *Phys. Rev. Lett.* **95** 083002
[19] Rohringer N and Santra R 2007 *Phys. Rev.* A **76** 033416
[20] Schlachter A S *et al* 2004 *J. Phys. B: At. Mol. Opt. Phys.* **37** L103
[21] Frasinski L J *et al* 1989 *Science* **246** 1029
[22] Santra R *et al* 2009 *Phys. Rev. Lett.* **103** 013002
[23] Inhester L 2013 *PhD Thesis* Göttingen
[24] Bozek J 2009 *Eur. Phys. J. Spec. Top.* **169** 129
[25] Bostedt C *et al* 2013 *J. Phys. B: At. Mol. Opt. Phys.* **46** 164003
[26] Mucke M *et al* 2012 *Rev. Sci. Instrum.* **83** 063106
[27] Eland J H D *et al* 2012 *Chem. Phys. Lett.* **548** 90
[28] Murphy B F *et al* 2014 *Nat. Commun.* **5** 4281
[29] Even U *et al* 2000 *J. Chem. Phys.* **112** 8068
[30] Hillenkamp M *et al* 2003 *J. Chem. Phys.* **118** 8699
[31] Foucar L *et al* 2012 *Comput. Phys. Commun.* **183** 2207
[32] Frasinski L J *et al* 2013 *Phys. Rev. Lett.* **111** 073002
[33] Zhaunerchyk V *et al* 2014 *Phys. Rev.* A **89** 053418
[34] Zhaunerchyk V *et al* 2013 *J. Phys. B: At. Mol. Opt. Phys.* **46** 164034
[35] Thompson M *et al* 1976 *Anal. Chem.* **48** 1336
[36] Tashiro M *et al* 2010 *J. Chem. Phys.* **132** 184302
[37] Cavell R G *et al* 1975 *J. Electron Spectrosc. Relat. Phenom.* **6** 281
[38] Frisch M J *et al* 2009 *Gaussian09 Revision D.01* (Wallingford, CT: Gaussian)
[39] Werner H J *et al* 1985 *J. Chem. Phys.* **82** 5053
[40] Löwdin P O 1966 *Quantum Theory of Atoms, Molecules, and the Solid State* (New York: Academic) A Tribute to John C Slater
[41] Werner H J *et al* 2012 *MOLPRO, Version 2012.1, a Package of ab initio Programs*
[42] Dunning T H Jr *et al* 1989 *J. Chem. Phys.* **90** 1007
[43] Woon D E *et al* 1993 *J. Chem. Phys.* **98** 1358
[44] Takahashi O *et al* 2011 *Chem. Phys.* **384** 28
[45] Tashiro M *et al* 2012 *J. Chem. Phys.* **137** 224306